Temperature Dependence of the Band Gap of CH 3 NH 3 PbI 3 Stabilized With PMMA: a Modulated Surface Photovoltage Study

ARTICLE *in* THE JOURNAL OF PHYSICAL CHEMISTRY C · OCTOBER 2015

Impact Factor: 4.77 · DOI: 10.1021/acs.jpcc.5b07132

THE JOURNAL OF PHYSICAL CHEMISTRY C

Article

pubs.acs.org/JPCC

Temperature Dependence of the Band Gap of $CH_3NH_3PbI_3$ Stabilized with PMMA: A Modulated Surface Photovoltage Study

Thomas Dittrich,* Celline Awino, Pongthep Prajongtat, Bernd Rech, and Martha Ch. Lux-Steiner

Institute of Heterogeneous Materials, Helmholtz-Center Berlin for Materials and Energy, Hahn-Meitner-Platz 1, D-14109 Berlin, Germany

Supporting Information

ABSTRACT: $CH_3NH_3PbI_3$ layers chemically stabilized with poly(methyl methacrylate) (PMMA), relevant for photovoltaic applications, have been investigated by modulated surface photovoltage (SPV) spectroscopy at temperatures (T) between −182 and 60 °C. SPV is sensitive only to the PMMA/$CH_3NH_3PbI_3$ interface region where photogeneration and charge separation take place. The T dependencies of the Tauc gap ($E_{g\text{-}Tauc}$, equivalent to absorption measurements) and of the gap determined from the maximum slope ($E_{g\text{-}tp}$, almost at increased absorption) were analyzed on the basis of the in-phase SPV spectra. At 32 °C, the values of $E_{g\text{-}Tauc}$ and $E_{g\text{-}tp}$ were 1.540 and 1.560 eV, respectively. A jump of $E_{g\text{-}Tauc}$ and $E_{g\text{-}tp}$ by 10 meV at 40 °C was interpreted as the transition from the tetragonal to the cubic phase at T lower than values known from literature. $E_{g\text{-}Tauc}$ and $E_{g\text{-}tp}$ of the cubic phase decreased with increasing T. In contrast, $E_{g\text{-}Tauc}$ and $E_{g\text{-}tp}$ of the tetragonal phase decreased moderately with decreasing T to 1.528 and 1.546 eV at −182 °C, respectively. No signature has been observed in $E_{g\text{-}Tauc}$ and $E_{g\text{-}tp}$ for the transition from the tetragonal to the orthorhombic phase. Structural interactions at PMMA/$CH_3NH_3PbI_3$ interfaces seem important for phase transitions in $CH_3NH_3PbI_3$ layers.

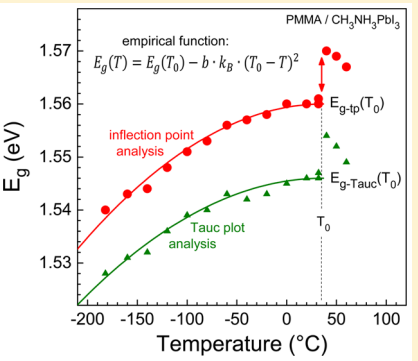

Methylammonium lead iodide ($CH_3NH_3PbI_3$) attracted extraordinary high attention in the past years as a photovoltaic absorber for high-efficiency solar cells.[1] Solvent engineering, interfaces, and temperature regimes are crucial for the development of highly efficient solar cells with $CH_3NH_3PbI_3$ absorbers. For example, solar energy conversion efficiencies above 18% have been achieved for solar cells based on $CH_3NH_3PbI_3$ by using hot-casting from solvents with high boiling point at temperatures above 100 °C.[2] The application of nanocomposites of $CH_3NH_3PbI_3$ with alumina or titania[3] and sophisticated solvent engineering[4] resulted in high efficiencies as well. Recently, the realization of tandem solar cells with a $CH_3NH_3PbI_3$ top cell has been demonstrated by employing a transparent contact system with large-area graphene.[5]

The band gap (E_g) and its temperature (T) dependence belong to the most fundamental properties of semiconductors. The knowledge of the precise T dependence of E_g of $CH_3NH_3PbI_3$ is not only of practical interest but also of fundamental interest regarding, for example, interactions of $CH_3NH_3PbI_3$ with different materials in contact regions.

Values of E_g of $CH_3NH_3PbI_3$ between 1.5 and 1.61 eV[6] have been reported and can sensitively depend on the preparation conditions and measurement techniques. To date, information about the temperature-dependent band gap of $CH_3NH_3PbI_3$ has been gained from photoluminescence (PL) measurements. As remark, the energy of the PL peak can depend also on the excitation intensity.[7] $CH_3NH_3PbI_3$ undergoes phase transitions from the tetragonal to the cubic phases at 327 K[8] and from the tetragonal to the orthorhombic phases at 162 K.[8] In the tetragonal phase, the $CH_3NH_3^+$ cation migrates toward the center of the perovskite cube, and the Pb−I2−Pb bond angle increases toward 180° with increasing temperature.[9] For $CH_3NH_3PbI_3$ single crystals, the energy of the PL peak of the tetragonal phase shifted, in contrast to conventional semiconductors, to higher photon energies with increasing temperature (about 1.54 eV at 160 K and 1.61 eV at 295 K[10]), whereas the PL peak of the orthorhombic phase shifted to higher photon energies with decreasing temperature.[10] A similar behavior was observed for $CH_3NH_3PbI_3$ layers[11] and for $CH_3NH_3PbI_3$ deposited on mesoporous TiO_2 electrodes.[12] Surprisingly, heating or cooling had a strong influence on the increase or decrease of the energy of the PL peak with increasing temperature of $CH_3NH_3PbI_3$ layers.[7] Further, decomposition or degradation of $CH_3NH_3PbI_3$ under vacuum[13] and/or at increased temperatures[14] can strongly influence defect formation and therefore the absorption near E_g.

$CH_3NH_3PbI_3$ layers can be prepared with a very low density of defects, with a sharp onset of absorption at the direct band gap and with a low degree of disorder. For example, the Urbach energy,[15] i.e., the energy describing the exponential absorption tails below the band gap, can be as low as 15 meV for $CH_3NH_3PbI_3$.[16] For comparison, the Urbach energy is above 50 meV for undoped amorphous silicon.[17]

The spectral range near E_g can be well studied by modulated surface photovoltage (SPV) spectroscopy.[18] SPV spectra can

Received: July 23, 2015
Revised: September 9, 2015

DOI: 10.1021/acs.jpcc.5b07132
J. Phys. Chem. C XXXX, XXX, XXX−XXX

also be measured in a quasi-static regime with a Kelvin probe.[19,20] However, quasi-static SPV measurements depend on any fast and slow processes such as charge separation, recombination, charge transport, trapping and detrapping, photochemical reactions, and so on. The precision of determining E_g is higher for modulated than for quasi-static SPV measurements since only the relatively fast electronic processes contribute to the signals. In addition, modulated in-phase SPV signals follow the modulation period and do therefore not depend directly on slow trapping and detrapping processes. Furthermore, modulated SPV spectroscopy is only sensitive to that region of a photovoltaic absorber where separation and diffusion of photogenerated charge carriers take place, i.e., to the region in solar cells being relevant for solar energy conversion.

The stability of $CH_3NH_3PbI_3$ over a wide temperature range for a long time is crucial for precise T-dependent studies of E_g by modulated SPV spectroscopy. Poly(methyl methacrylate) (PMMA) has been successfully used for stabilizing $CH_3NH_3PbI_3$ in solar cells (fast degradation started at 80 °C,[21] in combination with carbon nanotubes[22]). In this work, the stabilization of $CH_3NH_3PbI_3$ with PMMA allowed to study the T dependence of E_g between −182 and 60 °C.

Figure 1 shows the overview SPV spectra of the in-phase and phase-shifted by 90° SPV signals measured at 32 °C before

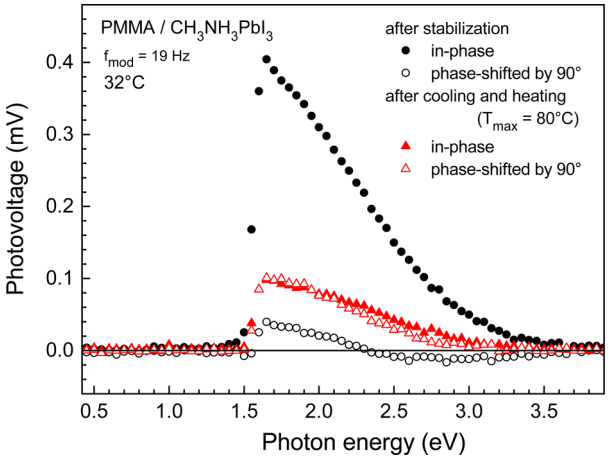

Figure 1. Overview SPV spectra of the in-phase (filled symbols) and phase-shifted by 90° (open symbols) SPV signals measured at 32 °C for the sample after stabilization (circles) and after cooling and heating cycles with a maximum temperature of 80 °C (triangles).

starting and after finishing the temperature-dependent measurements. All spectra show a sharp onset of signals between 1.5 and 1.6 eV, and no changes related to additional transitions such as PbI_2 have been detected.

Near E_g, the signs of the in-phase and phase-shifted by 90° SPV signals were positive, indicating that photogenerated electrons were preferentially separated toward the substrate and that partial trapping of photogenerated charge carriers lead to slow modulated charge separation with the opposite direction (see also ref 23).

The in-phase SPV signals reduced by about 4 times, whereas the phase-shifted by 90° SPV signals increased by more than 2 times after heating to 80 °C. This behavior was caused by degradation or defect generation in $CH_3NH_3PbI_3$ at high temperatures.

Figure 2a presents spectra of the in-phase and phase-shifted by 90° SPV signals measured at 32 °C. The onset energies of

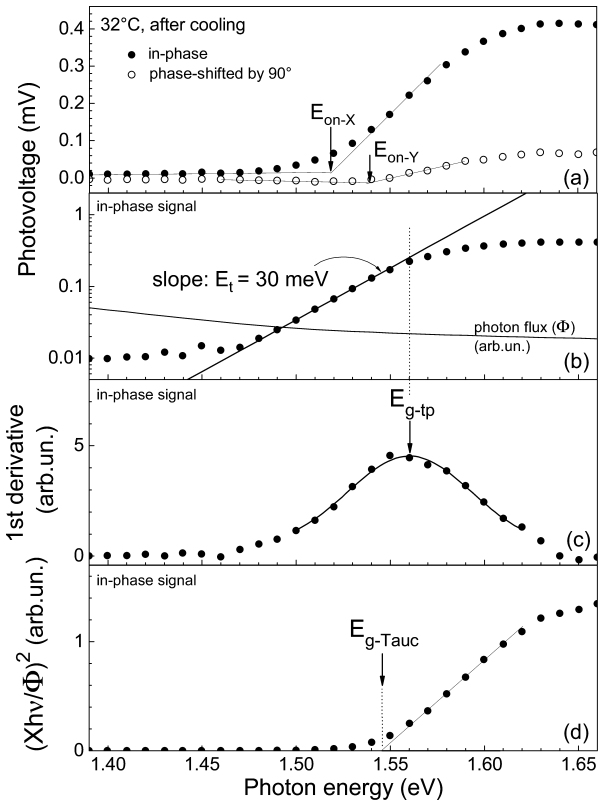

Figure 2. Spectra of the in-phase (filled circles) and phase-shifted by 90° (open circles) SPV signals measured around the band gap of $CH_3NH_3PbI_3$ at 32 °C (a), of the in-phase SPV signals on a logarithmic scale (b), of the first derivative of the in-phase SPV signals (c), and of the Tauc plot corresponding to the squared quotient of the x-signal and the photon flux (d). The solid lines in (a) describe the definitions of the onset energies ($E_{on\text{-}X}$ and $E_{on\text{-}Y}$). The thick and thin solid lines in (b) describe the slope of the exponential tails (E_t) and the photon flux, respectively. The solid lines in (c) and (d) describe the fit of the peak with a Gaussian giving the value of $E_{g\text{-}tp}$ at the peak position and the determination of the $E_{g\text{-}Tauc}$, respectively.

the in-phase and phase-shifted by 90° SPV signals ($E_{on\text{-}X}$ and $E_{on\text{-}Y}$, respectively) were determined from the intersection of the tangent in the inflection point and the baseline of the corresponding spectrum. For the given spectra, the values of $E_{on\text{-}X}$ and $E_{on\text{-}Y}$ were 1.518 and 1.539 eV, respectively.

Figure 2b shows the in-phase SPV signals on a logarithmic scale. The exponential increase of the SPV signal can be described by the energy of the band tails (E_t). As remark, E_t is not identical with the energy of the Urbach tail since excitation from a localized occupied into a localized unoccupied state is considered in optical but not necessarily in SPV measurements. The value of E_t amounted to 30 meV for the given spectrum which was larger than E_t for uncoated layers of $CH_3NH_3PbI_3$ (E_t ranged between 14 and 24 meV depending on preparation[23]) or for $CH_3NH_3PbI_3$ in a composite with nanoporous TiO_2 (E_t = 20 meV[23]). Therefore, the disorder was larger in $CH_3NH_3PbI_3$ layers coated with PMMA than in uncoated $CH_3NH_3PbI_3$ or in $TiO_2/CH_3NH_3PbI_3$ nanocomposite layers.

In comparison to optical absorption, SPV spectra can depend rather different on the photon energy near E_g, and it is useful to

DOI: 10.1021/acs.jpcc.5b07132
J. Phys. Chem. C XXXX, XXX, XXX−XXX

investigate the T dependence of E_g in spectral regions slightly above the direct band gap and closer to transitions related to defects near E_g. Therefore, two different values of E_g were determined from the in-phase SPV spectra by analyzing the inflection point ($E_{g\text{-}tp}$, value at almost increased absorption, Figure 2c) or by analyzing the Tauc plot[24] ($E_{g\text{-}Tauc}$, in analogy to optical absorption measurements, Figure 2d). The inflection point or maximum slope was obtained by fitting the first derivative of the in-phase SPV spectrum with one Gaussian. Despite the fact that $E_{g\text{-}tp}$ is slightly larger than E_g, the T dependencies of $E_{g\text{-}tp}$ and E_g should be nearly the same due to the steep onset of absorption at E_g. The analysis of Tauc plots of the in-phase SPV spectra presumed that the in-phase SPV signals were proportional to the absorption coefficient. This presumption was reasonable for the considered spectral range since the absorption length was much longer than the charge separation length, the character and the sign of the in-phase SPV signals did not change, and modulated SPV signals could be treated like small signals. The values of $E_{g\text{-}tp}$ and $E_{g\text{-}Tauc}$ were 1.560 and 1.546 eV, respectively, for the spectrum given in Figure 2.

The measurement regime is illustrated in Figure 3 showing the temperature dependencies of the maxima of the in-phase

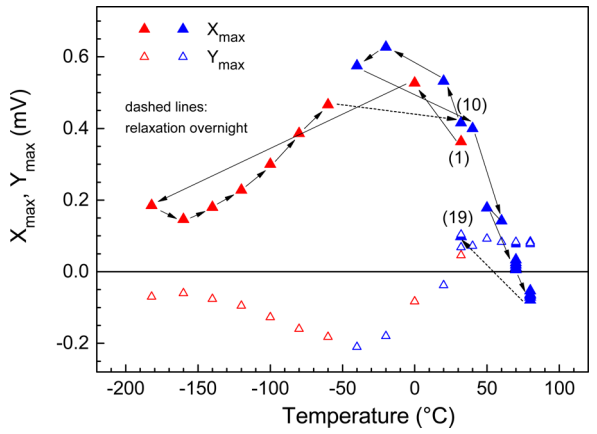

Figure 3. Temperature dependencies of the maxima of the in-phase (filled triangles, X_{max}) and phase-shifted by 90° (open triangles, Y_{max}) SPV signals. The arrows mark the regime of cooling or heating. The dashed arrows mark the relaxation overnight of X_{max} and Y_{max} to the initial temperatures after the measurements at low (red symbols) or high (blue symbols) temperatures (to points 10 or 19, respectively). Therefore, a reliable analysis of the in-phase SPV signals could be performed between −182 and 60 °C.

(X_{max}) and phase-shifted by 90° (Y_{max}) SPV signals. The temperature dependencies of X_{max} and Y_{max} followed common shapes independently of whether the signals were obtained in the low or high temperature cycles. The values of X_{max} and Y_{max} reached the maximum at −20 or −40 °C, respectively, whereas Y_{max} changed the sign between 20 and 32 °C. After the cycle at low temperatures (points 1−10 in Figure 3), the values of X_{max} and Y_{max} at 32 °C increased by about 20%; i.e., there was no degradation at low temperatures. For the cycle at high temperatures (points 10−19 in Figure 3), X_{max} reduced during continued measurements at 70 °C and changed to negative at 80 °C, giving evidence for ongoing degradation at the PMMA/$CH_3NH_3PbI_3$ interface.

The temperature dependencies of $E_{on\text{-}X}$, $E_{on\text{-}Y}$, $E_{g\text{-}tp}$, $E_{g\text{-}Tauc}$, and E_t are given in Figure 4. At temperatures below or equal

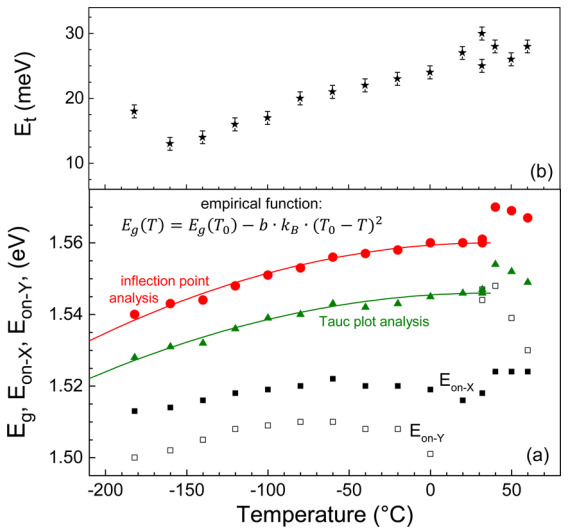

Figure 4. Temperature dependencies of $E_{on\text{-}X}$, $E_{on\text{-}Y}$, $E_{g\text{-}tp}$, and $E_{g\text{-}Tauc}$ ((a) filled squares, open squares, circles, and filled triangles, respectively) and of E_t (b). The solid lines describe the temperature dependencies of $E_{g\text{-}tp}$ and $E_{g\text{-}Tauc}$ below 30−40 °C by the empirical function (eq 1).

−20 °C, $E_{on\text{-}X}$ and $E_{on\text{-}Y}$ have similar temperature dependencies, whereas the values of $E_{on\text{-}X}$ were larger than the values of $E_{on\text{-}Y}$ by about 0.01 eV. $E_{on\text{-}X}$ increased from 1.520 eV at −20 °C to 1.522 eV at −60 °C and decreased to 1.513 eV at −182 °C. $E_{on\text{-}X}$ reached 1.516 eV at 20 °C, increased to 1.518 eV at 32 °C, and saturated at 1.524 eV for T above 32 °C. In contrast, $E_{on\text{-}Y}$ changed dramatically from 1.501 eV at 0 °C to 1.548 eV at 40 °C. This was caused by the change of the dominating modulated trapping and detrapping processes leading to a change of the sign of the phase-shifted by 90° SPV signals. Further, $E_{on\text{-}Y}$ decreased with increasing temperatures toward $E_{on\text{-}X}$.

$E_{g\text{-}tp}$ and $E_{g\text{-}Tauc}$ decreased monotonously with decreasing temperature at temperatures below or equal to 32 °C. $E_{g\text{-}tp}$ and $E_{g\text{-}Tauc}$ increased steeply by 0.01 eV between 32 and 40 °C and decreased to 1.569 at 50 °C and 1.567 at 60 °C. The steep increase of $E_{g\text{-}tp}$ and $E_{g\text{-}Tauc}$ between 32 and 40 °C shall be related to the phase transition from the tetragonal to the cubic phases at 54 °C.[8,25] It is known from literature that the transition temperature from the tetragonal to the cubic phases decreases with increasing pressure.[25] Therefore, the discrepancy between the transition temperatures measured for $CH_3NH_3PbI_3$ at normal pressure[8,25] and measured for $CH_3NH_3PbI_3$ coated with PMMA can be caused by an interaction between the PMMA and $CH_3NH_3PbI_3$ layers leading to an increase of stress in $CH_3NH_3PbI_3$. With respect to the phase diagram of $CH_3NH_3PbI_3$,[25] the stress between the PMMA and $CH_3NH_3PbI_3$ layers would be equivalent to a pressure between 200 and 300 MPa in the $CH_3NH_3PbI_3$ layer. Further, the values of E_t decreased monotonously with decreasing temperature from 24 meV at 0 °C to 13 meV at −160 °C but scattered between 25 and 30 meV in the temperature range between 20 and 60 °C which can be an additional indication for the change of stress at the PMMA/$CH_3NH_3PbI_3$ interface. Further, disorder can increase in the tetragonal phase of $CH_3NH_3PbI_3$ with increasing temperature due to the increased thermal motion of $CH_3NH_3^+$ cations and due to a continuous increase of the average Pb−I2−Pb bond angle toward 180°.[9] In addition, an increase of disorder can be

DOI: 10.1021/acs.jpcc.5b07132
J. Phys. Chem. C XXXX, XXX, XXX−XXX

caused by reorganization of domains in the photoferroic effect.[26]

The values of E_g above 32−40 °C can be related to the temperature dependence of E_g of the cubic phase of $CH_3NH_3PbI_3$. The decrease of E_g with increasing temperature by (1−2) × 10^{-3} eV/K between 40 and 60 °C seems reasonable for the cubic phase of $CH_3NH_3PbI_3$ in comparison to conventional semiconductors.[27]

The decrease of E_g of the tetragonal phase of $CH_3NH_3PbI_3$ with decreasing temperatures can be empirically described by a quadratic dependency:

$$E_g(T) = E_g(T_0) - bk_B(T_0 - T)^2 \quad (1)$$

where T_0 is the temperature of the phase transition from the cubic to the tetragonal phase (310 K has been chosen) and E_g can be $E_{g\text{-}tp}$ and $E_{g\text{-}Tauc}$ ($E_{g\text{-}tp}(T_0)$ and $E_{g\text{-}Tauc}(T_0)$ are equal to 1.560 and 1.546 eV, respectively), k_B is the Boltzmann constant (8.62 × 10^{-5} eV/K), and b is a free parameter (about 0.0055 and 0.0048 for $E_{g\text{-}tp}(T)$ and $E_{g\text{-}Tauc}(T)$).

No specific signature of E_g has been observed for the transition from the tetragonal to the orthorhombic phases at around −111 °C.[8,25] The increase of E_t from 13 meV at −160 °C to 18 meV at −182 °C gives evidence for an increase of disorder in $CH_3NH_3PbI_3$ with decreasing temperature in this range and might be an indication for a starting phase transition. The absence of a signature of the orthorhombic phase would not be surprising if taking into account that the orthorhombic phase of $CH_3NH_3PbI_3$ does not exist at pressures above 100 MPa[25] and that the reduced temperature of the phase transition from the tetragonal to the cubic phases of $CH_3NH_3PbI_3$ may be related to a pressure between 200 and 300 MPa. However, more detailed experiments in correlation with local phase transitions are required for getting a better understanding of the observed phenomena.

The anomalous behavior of the decrease of E_g of the tetragonal phase of $CH_3NH_3PbI_3$ with decreasing temperature is explained by the positive band gap deformation potential of these systems with respect to volume.[26] For the given temperature range, the change of E_g for the PMMA/$CH_3NH_3PbI_3$ system investigated by the surface/interface sensitive SPV was less by about 3 times in comparison to small (uncoated) single crystals of $CH_3NH_3PbI_3$ investigated by PL.[10] The lattice parameters perpendicular or along to the c-axis of the tetragonal phase of $CH_3NH_3PbI_3$ decrease or increase, respectively, and the rotation angle of the PbI_6 octahedron increases with decreasing temperature.[28] The corresponding increase of the Pb−I−Pb bond length along the c-axis with decreasing temperature and local variations in the rotation angle of the PbI_6 octahedron depend as well on the behavior of the $CH_3NH_3^+$ cation and of local stress. It can be supposed that the increase of the lattice constant along the c-axis with decreasing temperature is the reason for the anomalous behavior of the temperature dependence of E_g of the tetragonal phase of $CH_3NH_3PbI_3$ and that a reduced degree of freedom for local rotation of the PbI_6 octahedron may be the origin for changes in phase transitions toward the cubic phase at higher temperatures and toward the orthorhombic phase at lower temperatures. Sophisticated theoretical studies will be very useful for getting a better understanding about the temperature dependence of the band gap of free $CH_3NH_3PbI_3$ crystals and of $CH_3NH_3PbI_3$ in stacked layer systems such as PMMA/$CH_3NH_3PbI_3$.

EXPERIMENTAL METHODS

Glass substrates coated with molybdenum were subsequently cleaned in detergent, distilled water, acetone, and isopropanol using a sonicator for 15 min each. The samples were dried in nitrogen after each step. As remark, related substrates (thickness of molybdenum 0.5 μm) are used in conventional thin-film technology.

In a nitrogen-filled glovebox, precursors of $PbCl_2$ and CH_3NH_3I (molar ratio of 1:3; see for details ref 21) were spin-coated (2000 rpm for 10 s followed by 3000 rpm for 30 s) onto the substrates, and $CH_3NH_3PbI_3$ was formed during annealing at 100 °C for 60 min directly after the spin-coating. The local thickness of a $CH_3NH_3PbI_3$ layer was about 300 nm. Immediately after annealing, a hot solution of PMMA (40 mg of PMMA in 1 mL of butyl acetate[21] at 60 °C) was spin-coated (2000 rpm for 60 s) onto the $CH_3NH_3PbI_3$ layers. The $CH_3NH_3PbI_3$/PMMA samples were stabilized by storing in air for one month (see Supporting Information for more details). During this time, twin samples were permanently controlled by X-ray diffraction and SPV. No formation of PbI_2 has been observed during stabilization of $CH_3NH_3PbI_3$/PMMA in air.

Modulated SPV spectra were measured between −182 and +80 °C in a fixed capacitor placed into a homemade cryostat (base pressure 2 × 10^{-6} mbar). The modulated SPV signals (modulation frequency 19 Hz) were excited with a halogen lamp and a quartz prism monochromator (SPM2). The signals were detected with a high frequency buffer (input resistance 50 GΩ) and a double-phase lock-in amplifier (EG&G 5210). For control of the stability, the sample relaxed overnight to 32 °C after each of two distinct, partially overlapping in temperature, cycles at low and high temperature (−182 to 32 °C and −40 to 80 °C, respectively). In addition, two to four spectra were measured at each temperature.

ASSOCIATED CONTENT

Supporting Information

The Supporting Information is available free of charge on the ACS Publications website at DOI: 10.1021/acs.jpcc.5b07132.

Figure S1 (PDF)

AUTHOR INFORMATION

Corresponding Author

*E-mail dittrich@helmholtz-berlin.de; Ph +0049 30 806242090; Fax +0049 30 806243199 (T.D.).

Present Addresses

C.A. and B.R.: Institute for Silicon Photovoltaics, Helmholtz-Center Berlin for Materials and Energy, Kekuléstrasse 5, D-12489 Berlin, Germany.

P.P.: Department of Materials Science, Faculty of Science, Kasetsart University, Bangkok 10900, Thailand.

Funding

C.A. is supported by the KAAD (Katholischer Akademischer Austauschdienst).

Notes

The authors declare no competing financial interest.

REFERENCES

(1) see, for example Grätzel, M. The Light and Shade of Perovskite Solar Cells. *Nat. Mater.* **2014**, *13*, 838−842.

(2) Nie, W.; Tsai, H.; Asadpour, R.; Blancon, J.-C.; Neukirch, A. J.; Gupta, G.; Crochet, J. J.; Chhowalla, M.; Tretiak, S.; Alam, M. A.;

DOI: 10.1021/acs.jpcc.5b07132
J. Phys. Chem. C XXXX, XXX, XXX−XXX

Wang, H.-L.; Mohite, A. D. High-Effieincy Solution-Processed Perovskite Solar Cells with Millimeter-Scale Grains. *Science* **2015**, *347*, 522−525.
(3) Lee, M. M.; Teuscher, J.; Miyasaka, T.; Murakami, T. N.; Snaith, H. J. Efficient Hybrid Solar Cells Based on Meso-Superstructured Organometal Halide Perovskites. *Science* **2012**, *338*, 643−647.
(4) Jeon, N. M.; Noh, J. H.; Kim, Y. C.; Yang, W. S.; Ryu, S.; Seok, S. I. Solvent Engineering for High-Performance Inorganic-Organic Hybrid Perovskite Solar Cells. *Nat. Mater.* **2014**, *13*, 897−893.
(5) Lang, F.; Gluba, M. A.; Albrecht, S.; Rappich, J.; Korte, L.; Rech, B.; Nickel, N. Perovskite Solar Cells with Large-Area CVD-Graphene for Tandem Solar Cells. *J. Phys. Chem. Lett.* **2015**, *6*, 2745−2750.
(6) See, for example: Bretschneider, S. A.; Weickert, J.; Dorman, J. A.; Schmidt-Mende, L. Research Update: Physical and Electrical Characteristics of Lead Halide Perovskites for Solar Cell Applications. *APL Mater.* **2014**, *2*, 040701−1−040701−9.
(7) Wehrenfennig, C.; Liu, M.; Snaith, H. J.; Johnston, M. B.; Herz, L. M. Charge Carrier Recombination Channels in the Low-Temperature Phase of Organic-Inorganic Lead Halide Perovskite Films. *APL Mater.* **2014**, *2*, 081513-1−081513-10.
(8) Onoda-Yamamuro, N.; Matsuo, T.; Suga, H. Calorimetric and IR Spectroscopy Studies of Phase Transitions in Methylammonium Trihalogenoplumbates (II). *J. Phys. Chem. Solids* **1990**, *51*, 1383−1395.
(9) Weller, M. T.; Weber, O. J.; Henry, O. F.; Di Pumpo, A. M.; Hansen, T. C. Complete Structure and Cation Orientation in the Perovskite Photovoltaic Methylammonium Lead Iodide between 100 and 352 K. *Chem. Commun.* **2015**, *51*, 4180−4183.
(10) Fang, H.-H.; Raissa, R.; Abdu-Aguye, M.; Adjotatse, S.; Blake, G. R.; Even, J.; Loi, M. A. Photophysics of Organic-Inorganic Hybrid Lead Iodide Perovskite Single Crystals. *Adv. Funct. Mater.* **2015**, *25*, 2378−2385.
(11) Wu, K.; Bera, A.; Ma, C.; Du, Y.; Yang, Y.; Li, L.; Wu, T. Temperature Dependent Excitonic Photoluminescence of Hybrid Organometal Halide Perovskite Films. *Phys. Chem. Chem. Phys.* **2014**, *16*, 22476−22481.
(12) Yamada, Y.; Nakamura, T.; Endo, M.; Wakamiya, A.; Kanemitsu, Y. Near-Band-Edge Optical Responses of Solution-Processed Organic-Inorganic Hybrid Perovskite $CH_3NH_3PbI_3$ on Mesoporous TiO_2 Electrodes. *Appl. Phys. Express* **2014**, *7*, 032302-1−032302-4.
(13) Deretzis, I.; Alberti, A.; Pellegrino, G.; Smecca, E.; Giannazzo, F.; Sakai, N.; Miyasaka, T.; La Magna, A. Atomistik Origins of $CH_3NH_3PbI_3$ degradation to PbI_2 in Vacuum. *Appl. Phys. Lett.* **2015**, *106*, 131904-1−131904-4.
(14) Supasai, T.; Rujisamphan, N.; Ullrich, K.; Chemseddine, A.; Dittrich, T. Formation of a Passivating $CH_3NH_3PbI_3/PbI_2$ Interface During Moderate Heating of $CH_3NH_3PbI_3$ Layers. *Appl. Phys. Lett.* **2013**, *103*, 183906-1−183906-3.
(15) Urbach, F. The Long-Wavelength Edge of Photographic Sensitivity and of the Electronic Absorption of Solids. *Phys. Rev.* **1953**, *92*, 1324.
(16) De Wolf, S.; Holovsky, J.; Moon, S.-J.; Löper, P.; Niesen, B.; Ledinsky, M.; Haug, F.-J.; Yum, J.-H.; Ballif, C. Organometallic Halide Perovskites: Sharp Optical Absorption Edge and Its Relation to Photovoltaic Performance. *J. Phys. Chem. Lett.* **2014**, *5*, 1035−1039.
(17) Stutzmann, M. The Defect Density of Amorphous Silicon. *Philos. Mag. B* **1989**, *60*, 531−546.
(18) Duzhko, V.; Timoshenko, V.; Yu; Koch, F.; Dittrich, Th. Photovoltage in Nanocrystalline Porous TiO_2. *Phys. Rev. B: Condens. Matter Mater. Phys.* **2001**, *64*, 075204-1−075204-7.
(19) Lagowski, J.; Baltov, I.; Gatos, H. C. Surface Photovoltage Spectroscopy and Surface Piezoelectric Effect in GaAs. *Surf. Sci.* **1973**, *40*, 216−226.
(20) Kronik, L.; Shapira, Y. Surface Photovoltage Phenomena: Theory, Experiment, and Applications. *Surf. Sci. Rep.* **1999**, *37*, 1−206.
(21) Yu, H.; Wang, F.; Xie, F.; Li, W.; Chen, J.; Zhao, N. The Role of Chlorine in the Formation Process of "$CH_3NH_3PbI_{3-x}Cl_x$" Perovskites. *Adv. Funct. Mater.* **2014**, *14*, 7102−7108.
(22) Habisreutinger, S. N.; Leijtens, T.; Eperon, G. E.; Stranks, S. D.; Nicholas, R. J.; Snaith, H. J. Carbon Nanotube/Polymer Composites as a Highly Stable Hole Collection Layer in Perovskite Solar Cells. *Nano Lett.* **2014**, *14*, 5561−5568.
(23) Prajongtat, P.; Dittrich, Th. Precipitation of $CH_3NH_3PbCl_3$ in $CH_3NH_3PbI_3$ and Its Impact on Modulated Charge Separation. *J. Phys. Chem. C* **2015**, *119*, 9926−9933.
(24) Tauc, J. Optical Properties and Electronic Structure of Amorphous Ge and Si. *Mater. Res. Bull.* **1968**, *3*, 37−46.
(25) Gesi, K. Effect of Hydrostatic Pressure on the Structural Phae Transitions in $CH_3NH_3PbX_3$ (X = Cl, Br, I). *Ferroelectrics* **1997**, *203*, 249−268.
(26) Frost, J. M.; Butler, K. T.; Brivio, F.; Hendon, C. H.; van Schilfgaarde, M.; Walsh, A. Atomomistic Origins of High-Performance in Hybrid Halide Perovskite Solar Cells. *Nano Lett.* **2014**, *14*, 2584−2590.
(27) Varshni, Y. P. Temperature Dependence of the Band Gap in Semiconductors. *Physica* **1967**, *34*, 149−154.
(28) Kawamura, Y.; Mashiyama, H.; Hasebe, K. Structural Study on Cubic-Tetragonal Transition of $CH_3NH_3PbI_3$. *J. Phys. Soc. Jpn.* **2002**, *71*, 1694−1697.

DOI: 10.1021/acs.jpcc.5b07132
J. Phys. Chem. C XXXX, XXX, XXX−XXX